Mathematical Models and Methods in Applied Sciences
Vol. 9, No. 4 (1999) 513–539

MATHEMATICAL MODELLING OF MACROPHAGE DYNAMICS IN TUMOURS

MARKUS R. OWEN*
Department of Mathematics, University of Utah, Salt Lake City, UT 84112, USA

JONATHAN A. SHERRATT†
Department of Mathematics, Heriot-Watt University, Edinburgh EH14 4AS, UK

Communicated by N. Bellomo and M. Chaplain
Received 9 March 1998

Macrophages form an important part of the immune response to cancer. In this paper, we present a mathematical model of reaction–diffusion form, which represents the influx of macrophages into a small avascular tumour, and their dynamics within the tumour as it grows. The model predicts that, despite their ability to selectively kill tumour cells, macrophages are unable to prevent tumour growth. However, significant effects on the form of the tumour are predicted, including in particular the formation of spatial patterns. When the model is extended to include macrophage chemotaxis, these patterns can in some cases bifurcate to give irregular spatiotemporal oscillations, and the authors present a detailed numerical bifurcation study which suggests a novel dynamical origin for these oscillations. Finally, we present results of model simulations in two spatial dimensions.

1. Introduction

Macrophages form an important part of the immune response to cancer. They are the mature form in tissue of a type of white blood cell known as a monocyte, and are recruited to tumour sites by attracting gradients of chemicals produced by tumour cells. This recruitment can be very effective: for example, in many cases of breast carcinoma, macrophages constitute over 50% of the total cell mass.[37] The role of macrophages within tumours is complex. They are known to selectively kill tumour cells,[33] but can also promote tumour growth by encouraging vascularisation.[30] These various processes will be explained more fully later in the paper; for more detailed biological reviews, see Refs. 18, 24 and 32.

In this paper, we consider the effect of macrophage-mediated killing of tumour cells during the early, avascular stage of tumour growth. This process is

*E-mail: owen@math.utah.edu
†E-mail: jas@ma.hw.ac.uk

initiated when a cell in the tissue undergoes a mutation, giving it a proliferative advantage over its normal counterparts[53]; mathematical models for this process were given in Refs. 46 and 54. The avascular phase of growth terminates because of the limited rate at which nutrients can diffuse into a solid tumour,[23] and thereafter the tumour becomes quiescent; this diffusion-limited cessation of growth was the first area of tumour biology to be modelled mathematically[1,11,22] and recent modelling has clarified the effects of tumour shape on the process.[12,52] Tumour growth is then resumed via the onset of angiogenesis,[21] in which tumours acquire their own blood supply, leading to unconstrained (and potentially lethal) growth; for models of the angiogenic process, see Refs. 13 and 14. Subsequent metastasis, leading to secondary tumours, requires the development of invasive tumour cell phenotypes; for modelling of tumour invasion, see Ref. 40.

Previous mathematical models of tumour immunology fall into two main categories, using either generic representations of the immune response[2,4,25,46] or detailed models focussing on particular aspects of immune cell–tumour cell interactions[27,28] (see Ref. 3 or other papers in this issue for review). Our approach falls in between these categories of model: we focus specifically on macrophages, and use equations that are based at least qualitatively on known details of macrophage–tumour interactions; however, we keep our modelling sufficiently simple that we can consider the effects of macrophages within the context of a tumour that is growing in space. In the next section, we describe our model, and in Sec. 3, we discuss the form of model solutions in the absence of spatial variation, including the use of the model to study macrophage-based immunotherapy. In Sec. 4, we discuss model solutions in one spatial dimension, showing that macrophages are able to induce spatial patterning within the growing tumour. We extend the model in Sec. 5 to include explicit macrophage chemotaxis, and show that this can induce spatiotemporal irregularities within the tumour. Finally in Sec. 6, we present numerical simulations of the model in two spatial dimensions. Our model has been presented previously in Ref. 38, and preliminary results on spatial patterning were given in Ref. 39. The central contribution of this paper is a detailed study of the development of both regular and irregular spatial patterns.

2. Model Development

Our model restricts attention to the interactions between mutant cells, normal tissue, macrophages, and their chemical regulators. We make the simplifying assumption that there is a single chemical regulator responsible for activation of macrophages, control of their proliferation, and stimulation of their influx from the bloodstream. In reality, many different chemicals are involved, including tumour necrosis factor,[31] macrophage colony stimulating factor[41] and members of the monocyte chemotactic protein family[10,49]; however, all these regulators derive primarily from mutant cells, and can be treated together to a first approximation.

Activation and inhibition of mutant and normal cell growth are not included in our model; instead we represent the proliferative advantage of mutant cells in

terms of an increased basic growth rate. Thus the variables we consider are the densities of macrophages, $l(\mathbf{x},t)$; mutant cells, $m(\mathbf{x},t)$; normal cells, $n(\mathbf{x},t)$; macrophage-mutant cell complexes, $c(\mathbf{x},t)$; and the concentration of the chemical regulator, $f(\mathbf{x},t)$. In the following sections we will outline the assumptions and interactions relevant to each species, and give mathematical descriptions in terms of differential equations.

2.1. *Macrophages*

Macrophages destroy tumour cells by binding to form a complex and then lysing the mutant cell; direct cell-cell contact is an essential part of this process.[26] Quiescent macrophages must be biochemically activated before complex formation and lysis are possible.[24,32] We assume that the rate of complex formation is linear with respect to chemical concentration, and macrophage and tumour cell densities. In addition we assume that the complex returns viable macrophages after lysis of the mutant cell.[18] Note that the source of regulators is mutant cells. Schematically this can be represented in the following form:

$$f + l + m \xrightarrow{k_1} c + f, \quad c \xrightarrow{k_2} l + \text{debris}.$$

Here k_1 and k_2 are positive constants. It is important to stress that there is no definitive experimental data on the details of this tumour cell destruction; we have considered various alternative formulations for this process, such as separating the activation and complex formation steps, but such changes do not significantly alter the qualitative model behaviour.

The remaining assumptions that we make with regard to macrophages are: (i) they have spatially random motion combined with movement up gradients in the concentration of chemical regulator; (ii) they proliferate only in the presence of the chemical regulator,[8] and such proliferation increases linearly with the concentration; (iii) their proliferation is limited by the crowding effect of all cell types; (iv) there is an influx from capillaries, which, due to chemotaxis, increases linearly with regulator concentration; and (v) they die with some constant rate per cell. In the absence of chemical regulator, the normal background level of tissue macrophages is maintained by a constant influx, at a rate denoted by I.

We use a term for proliferation of macrophages of the form:

$$\text{(chemical concentration)} \times \text{(macrophage density)} \times \text{(crowding term)}.$$

The most common representation of crowding effects on cell division is the logistic term, $r(x) = (k - x)$, which has been used in modelling a wide range of biological systems.[20,45] In this case it is inappropriate, since the logistic crowding term can be negative, which does not make sense when it is multiplied by the chemical concentration — macrophage death should not be promoted. Therefore we use the term $r(x) = (N + N_e)/(N + x)$, where N_e is the equilibrium cell density in normal tissue and N is a measure of crowding response. There is no particular significance

in this choice of functional form; in the absence of detailed biological data, only the qualitative form of the function is known.

Combining these terms gives the following conservation equation for macrophages:

$$\frac{\partial l}{\partial t} = \overbrace{D_l \nabla^2 l - \chi_l \nabla(l \nabla f)}^{\text{cell migration}} + \overbrace{\frac{\alpha f l (N + N_e)}{N + l + m + n}}^{\text{proliferation}} + \overbrace{I(1 + \sigma f)}^{\text{influx}} - \overbrace{k_1 f l m + k_2 c}^{\text{lysis}} - \overbrace{\delta_l l}^{\text{death}} . \quad (1)$$

2.2. *Mutant and normal cells*

Most tumours arise initially from a mutation that affects the control of cell division, giving the mutant cell a proliferative advantage over its peers.[53] Such mutations have been the subject of previous detailed models,[46,54] but here our focus is on the role of macrophages during the early stages of tumour growth, and thus we use a very simple model. Specifically, we assume that the dynamics of mutant and normal cells are alike except for the removal of mutant cells by macrophages, and a scaling of the mutant cell growth rate by $\xi > 1$ to model their proliferative advantage. We use the same crowding term as discussed above, and a growth rate in normal tissue of δ, balanced by an equal rate of cell death, so that combining these elements with diffusion to simulate random cell migration gives the following conservation equations for mutant and normal cells:

$$\begin{aligned} \frac{\partial m}{\partial t} &= \overbrace{D_m \nabla^2 m}^{\text{cell migration}} + \overbrace{\frac{\xi \delta m (N + N_e)}{N + l + m + n}}^{\text{proliferation}} - \overbrace{\delta m}^{\text{death}} - \overbrace{k_1 f l m}^{\text{lysis}}, \\ \frac{\partial n}{\partial t} &= D_n \nabla^2 n + \frac{\delta n (N + N_e)}{N + l + m + n} - \delta n . \end{aligned} \quad (2)$$

2.3. *Chemical regulation and cell lysis*

Chemotaxis, macrophage proliferation, and mutant cell lysis are the important interactions considered in this model, and all are stimulated by chemicals produced by mutant cells, which we are representing as a single generic regulator $f(\mathbf{x}, t)$, whose sole source is mutant cells. We assume a constant secretion rate β per unit of mutant cell density, and a linear natural decay with rate δ_f. The complex density is also assumed to decay linearly, with rate δ_c. Including random motion and the binding and lysis terms discussed above completes the derivation of our model:

$$\begin{aligned} \frac{\partial f}{\partial t} &= \overbrace{D_f \nabla^2 f}^{\text{diffusion}} + \overbrace{\beta m}^{\text{prod}^n} - \overbrace{\delta_f f}^{\text{decay}} , \\ \frac{\partial c}{\partial t} &= \overbrace{D_c \nabla^2 c}^{\text{migration}} + \overbrace{k_1 f l m - k_2 c}^{\text{lysis}} - \overbrace{\delta_c c}^{\text{death}} . \end{aligned} \quad (3)$$

2.4. *Non-dimensionalisation*

Equations (1)–(3) are non-dimensionalised using the following rescalings, where L is half a typical cell length, and f_0 is a typical concentration of chemical regulator:

$$t^* = \delta t, \quad x^* = \frac{x}{L}, \quad l^* = \frac{l}{N_e}, \quad m^* = \frac{m}{N_e}, \quad n^* = \frac{n}{N_e}, \quad c^* = \frac{c}{N_e}, \quad f^* = \frac{f}{f_0},$$

$$D_l^* = \frac{D_l}{\delta L^2}, \quad \chi_l^* = \frac{\chi_l f_0}{\delta L^2}, \quad D_m^* = \frac{D_m}{\delta L^2}, \quad D_n^* = \frac{D_n}{\delta L^2}, \quad D_f^* = \frac{D_f}{\delta L^2}, \quad D_c^* = \frac{D_c}{\delta L^2},$$

$$\alpha^* = \frac{\alpha f_0}{\delta}, \quad N^* = \frac{N}{N_e}, \quad I^* = \frac{I}{N_e \delta}, \quad \sigma^* = f_0 \sigma, \quad k_1^* = \frac{k_1 f_0 N_e}{\delta},$$

$$k_2^* = \frac{k_2}{\delta}, \quad \delta_l^* = \frac{\delta_l}{\delta}, \quad \delta_f^* = \frac{\delta_f}{\delta}, \quad \delta_c^* = \frac{\delta_c}{\delta}, \quad \beta^* = \frac{\beta N_e}{f_0 \delta}.$$

Recall that N_e is the equilibrium cell density in normal tissue. Applying these rescalings, and dropping the asterisks for notational simplicity, gives:

$$\frac{\partial l}{\partial t} = D_l \nabla^2 l - \chi_l \nabla(l \nabla f) + \frac{\alpha f l (N+1)}{N + l + m + n} + I(1 + \sigma f) - k_1 f l m + k_2 c - \delta_l l, \quad \text{(4a)}$$

$$\frac{\partial m}{\partial t} = D_m \nabla^2 m + \frac{\xi m (N+1)}{N + l + m + n} - m - k_1 f l m, \quad \text{(4b)}$$

$$\frac{\partial n}{\partial t} = D_n \nabla^2 n + \frac{n(N+1)}{N + l + m + n} - n, \quad \text{(4c)}$$

$$\frac{\partial f}{\partial t} = D_f \nabla^2 f + \beta m - \delta_f f, \quad \text{(4d)}$$

$$\frac{\partial c}{\partial t} = D_c \nabla^2 c + k_1 f l m - k_2 c - \delta_c c. \quad \text{(4e)}$$

The experimental data available for parameter estimation is limited, but enables order of magnitude estimates to be obtained for most of the parameters, and details of this were given in Ref. 38 for the kinetic parameters, and in Ref. 39 for motility parameters.

3. Spatially Independent Solutions

The majority of this paper is focussed on spatially varying solutions, but as an essential precursor to this work, we discuss in this section solutions of the spatially homogeneous system given by setting $D_l = \chi_l = D_m = D_n = D_f = D_c = 0$. In the resulting system of ordinary differential equations, there are four types of steady state to consider. The first two are somewhat trivial: a macrophage-only state $l = I/\delta_l$, $m = n = f = c = 0$, and the normal tissue state, consisting of normal cells and macrophages: $l = I/\delta_l$, $m = 0$, $n = 1 - I/\delta_l$, $f = c = 0$. Straightforward linear stability analysis shows that both these steady states are unstable to the introduction of mutant cells.

The third type of steady state is that of a tumour with no normal cells remaining, denoted the mutant-only steady state, and the fourth steady state is of mixed type, with all cell species coexisting. Real tumours certainly contain a variety of cell types,[32] and other models[46,54] also predict this type of solution. If the growth advantage of mutant cells is too high, coexistence is not possible, and steady states of this type cannot exist. Figure 1 illustrates the way in which these last two steady states change with σ, the macrophage influx parameter. We have identified a number of bifurcation points, at which the number and stability of steady states change. This is discussed in some detail in Ref. 38; for the purposes of this paper the key result is that, with respect to homogeneous perturbations, at least one tumour steady state is stable, and that for realistic parameter ranges there is only a very small region of parameter space in which both coexistence and mutant-only steady states are stable.

Numerical simulations of the ordinary differential equation model given by setting $D_l = \chi_l = D_m = D_n = D_f = D_c = 0$ suggest that when only one steady state is locally stable, it is also globally stable for positive solutions; in the small regions of parameter space where two tumour steady states are both locally stable, solutions evolve to one or the other of these, depending on initial conditions. In particular, this implies that introduction of a small mutant cell density to the normal tissue state causes the solution to evolve to a tumour steady state. This occurs despite the presence of cytotoxic macrophages, because the macrophage immune response is second order in the density of mutant cells. By this, we mean that as well as having an explicit dependence on the mutant cell density m, the immune

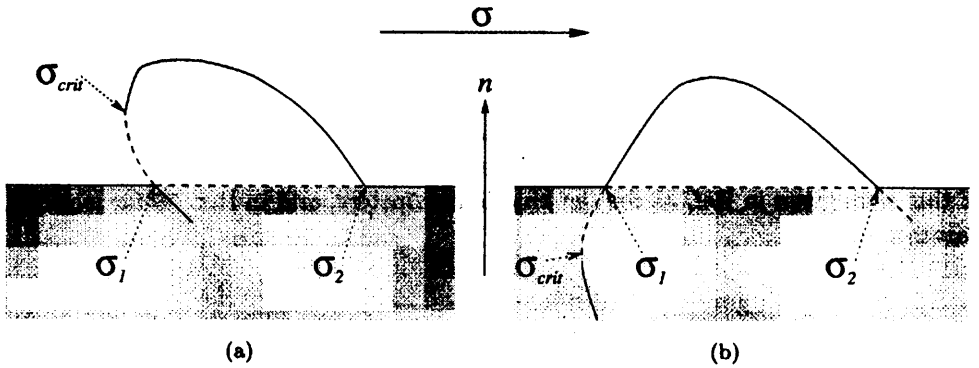

Fig. 1. Schematic representation of the bifurcation structures for the homogeneous tumour steady states of the dimensionless model (4). Solid lines indicate stability, dashed lines instability. The bifurcation parameter σ is the measure of the increase in macrophage influx from the bloodstream in response to chemoattractants secreted by tumour cells. Tumour steady states of the model (4) are of two types: (i) mutant-only ($n = 0$), where no normal cells survive, indicated by the horizontal lines in the diagram; (ii) coexistence ($n \neq 0$), where normal cells continue to proliferate along with mutant cells, indicated by the curves. We do not consider coexistence steady states with negative cell densities, corresponding to those in the shaded area $n < 0$. There are two types of bifurcation structure, which depend upon the nature of the coexistence steady state at $\sigma = \sigma_c$: (a) $n|_{\sigma=\sigma_c} > 0$, (b) $n|_{\sigma=\sigma_c} < 0$.

response term $-k_1 flm$ also depends on the concentration of chemical regulator f, whose production rate is itself dependent on the mutant cell density.

Before we go on to discuss spatially varying solutions, we mention briefly the application of the temporal (ordinary differential equation) model to macrophage based immunotherapies, which have been used in a number of trials, and are of two main types. Some current adoptive treatments remove circulating blood monocytes, mature and activate them in culture with interferon-γ, and re-introduce what are now macrophages into the patient.[7] Our model would need to explicitly include activated macrophages to be applicable here. The second main type is the local or systemic administration of macrophage activating chemicals, such as MTP-PE,[19] a

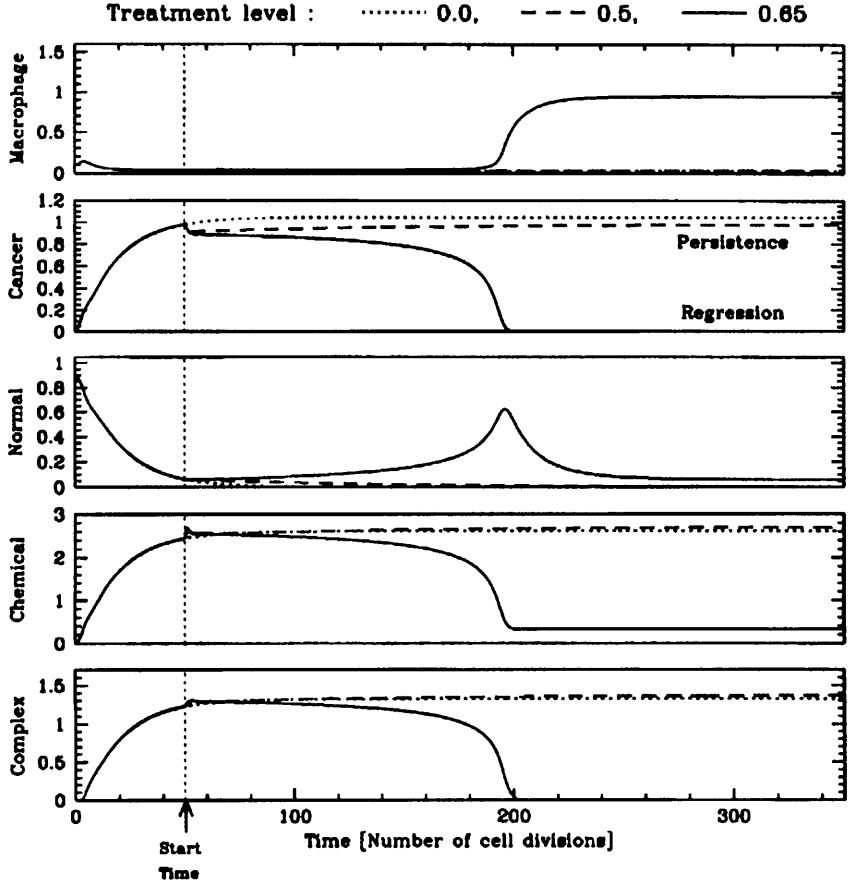

Fig. 2. Model simulations of the effect of exogenous addition of chemical regulator. Solutions are shown for the control case and for two different rates of chemical addition. The dimensionless treatment start time is 50. When the treatment level is sufficiently high, the tumour regresses. The solutions are obtained by solving the ODEs given by putting $D_l = \chi_l = D_m = D_n = D_f = D_c = 0$ in (4), and adding a constant to Eq. (4d). The parameters are $\alpha = 0.01$, $\beta = 5.0$, $\delta_c = 0.5$, $\delta_f = 2.0$, $\delta_l = 0.1$, $N = 1$, $I = 0.01$, $k_1 = 10.0$, $k_2 = 0.2$, $\sigma = 25$, $\xi = 2.0$, and the initial conditions are $(l, m, n, f, c) = (0.1, 0.001, 0.9, 0, 0)$.

synthetic analogue of a component of the bacterial cell wall, and lymphokines, such as[5] interleukin-2 and interferon-γ.[6] Our model is able to directly simulate this latter type of therapy, by adding a constant to the right-hand side of the f in Eq. (4d), representing exogenous addition of chemical regulator. Crucially, this change results in the macrophage removal of tumour cells becoming first order in mutant cell density, since the production of chemical regulator f now has a component which is independent of that density. When the rate of chemical addition is sufficiently large, the steady state structure of the model changes so that both normal tissue and tumour steady states are stable. This is illustrated in Fig. 2, where we plot model solutions without exogenous chemical addition, and with such addition at two different rates; at the larger rate of addition, the macrophage cytotoxicity is sufficient to eliminate the mutant cells. A significant prediction of such simulations is that the time at which treatment is started is a key factor in its efficacy. One important role for the type of mathematical modelling we describe is to enable prediction of optimal therapeutic regimes in particular cases; however, more detailed parameter estimates would be required to make this possible.

4. Wave Front Solutions and Spatial Patterns

Real tumours *in vivo* are nearly always spatially heterogeneous, often with no apparent order whatsoever. This should be no surprise given the varied environment in which tumours grow, and the wide variety of interactions with different cell types and tissue structures. Such spatial variations can arise from a variety of biological mechanisms, which include convection and mechanical stress due to movement of the underlying tissue structures, and heterogeneities in the underlying tissue itself. These features do not relate specifically to the macrophage–tumour interaction, and are not considered in our model, although they may be very significant. However, we will show that spatial variations can arise simply as a consequence of cell movement and chemical diffusion, within the context of the macrophage–tumour interaction. In this section, we discuss the implications of purely random motility of cells and diffusion of the chemical regulator, that is we assume $\chi_l = 0$; we demonstrate the existence of travelling wave solutions, and the possibility of spatial patterning within the tumour. In Sec. 5, we go on to consider the effect of nonzero χ_l.

We are concerned with the evolution of model solutions following a spatially localised introduction of mutant cells to an infinite domain on which the system is at the normal tissue steady state. In a wide range of numerical simulations, we have found that provided the chemical diffusion coefficient D_f is sufficiently small, this results in a travelling wave solution originating from the site of mutation, with either the coexistence or mutant-only tumour steady state behind the wave, depending on the kinetic parameters. Figure 3 illustrates such a simulation, with parameters such that the stable homogeneous steady state, and hence the state behind the wave, is of coexistence type. Linear analysis of the travelling wave ODEs corresponding to (4) suggests that the wave speed is given by $2[D_m(\xi - 1)]^{1/2}$,[39] and extensive numerical simulations of the PDEs support this. Using our estimated parameter

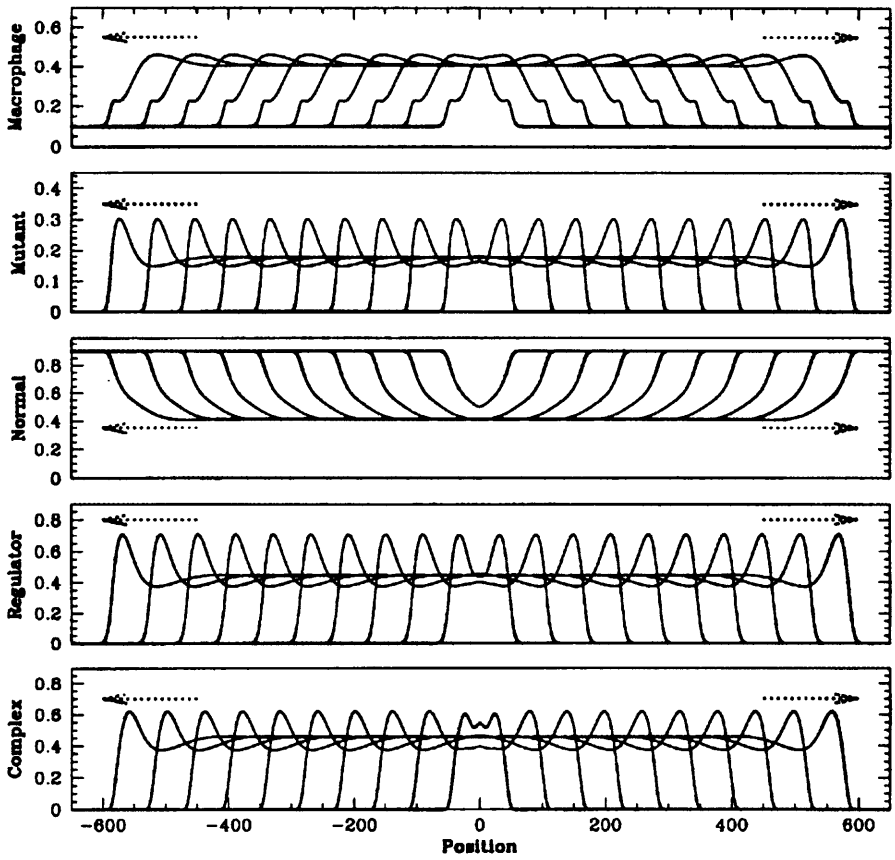

Fig. 3. Numerical simulation in one dimension of the dimensionless model (4), with no macrophage chemotaxis ($\chi_l = 0$), showing the evolution from a localised mutation at the centre. The initial conditions were the normal tissue steady state $l = 0.1, m = 0, n = 0.9, f = 0, c = 0$ on the whole domain, apart from the mutation $l = 0, m = 1, n = 0, f = 0, c = 0$ for $-0.5 < x < 0.5$. A travelling wave is established as the tumour grows, with the composition behind the wave front that of the homogeneous stable steady state, which depends on the kinetic parameters. In this case the coexistence steady state is stable. The solution is plotted at intervals of 10 dimensionless time units, up to a final time of 100, at which point the numerically calculated wave speed = 6.007 38, compared to the predicted speed of $2[D_m(\xi - 1)]^{1/2} = 6$, a difference of less than 0.005%. This corresponds to a dimensional speed of 1.2×10^{-10} ms^{-1} ≈ 0.01 mm day^{-1}. The parameters are: $D_l = D_m = D_n = 5$, $D_f = 30$, $D_c = 2.5, \alpha = 0.01$, $\beta = 5.0$, $\delta_c = 0.5$, $\delta_f = 2.0$, $\delta_l = 0.1$, $N = 1$, $I = 0.01$, $k_1 = 10.0$, $k_2 = 0.2$, $\sigma = 58$, $\xi = 2.8$.

values, this gives a dimensional wave speed of the order of 10^{-10} ms^{-1}, indicating that it would take about 100 days for a tumour to grow to a size of 1 mm.

These results show that the macrophage population has no effect on the speed of tumour growth; however, the macrophages do have a significant effect on tumour composition, because of their effect on the homogeneous steady states. Moreover, when the chemical diffusion coefficient D_f increases above a critical value, numerical simulations of the model predict a much more significant effect on tumour

composition, with a spatial pattern developing behind the advancing wave front, as illustrated in Fig. 4. Note that the pattern is stationary behind the wave, growing in extent but not changing in form or location. Such regular patterns are of course not observed in the stochastic inhomogeneous environment of a real tumour, but their observation in model solutions suggests that the macrophage–tumour interaction may be a first step towards the more irregular spatial inhomogeneities seen in the real situation.

This pattern formation is an example of a Turing mechanism.[36] However, there is no prepattern involved: in this case the mutant cells are the local activator, and

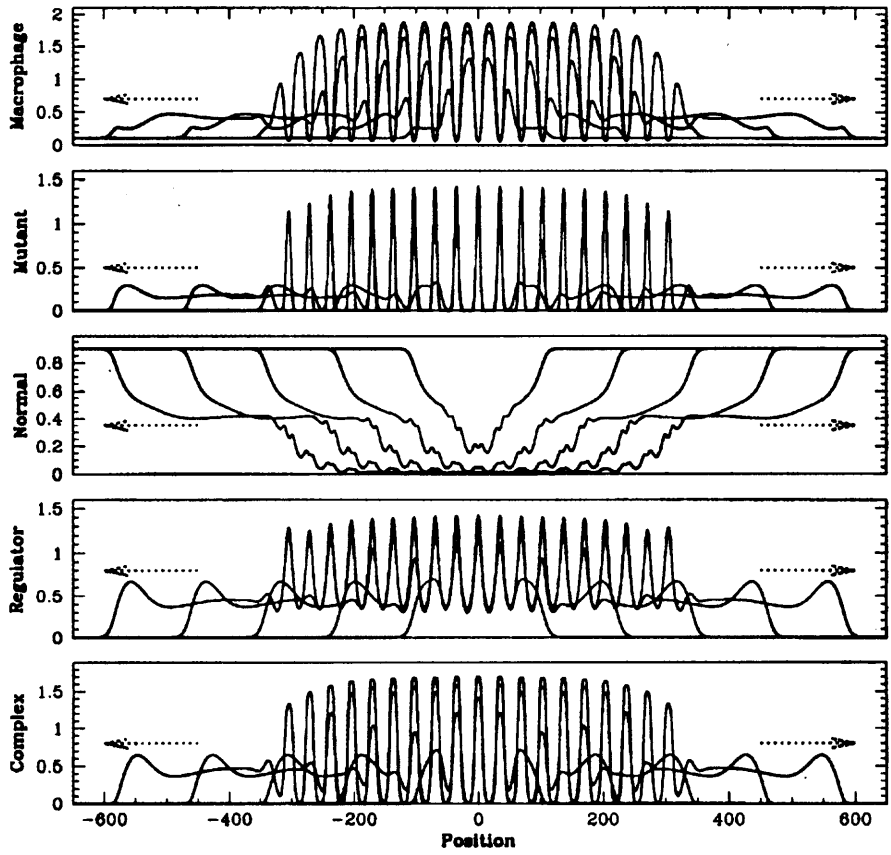

Fig. 4. Numerical simulation in one dimension of the model (4), with no macrophage chemotaxis ($\chi_l = 0$), showing the evolution from a localised mutation at the centre. The initial conditions were the normal tissue steady state $l = 0.1, m = 0, n = 0.9, f = 0, c = 0$ on the whole domain, apart from the mutation $l = 0, m = 1, n = 0, f = 0, c = 0$ for $-0.5 < x < 0.5$. The solution is shown at intervals of 20 dimensionless time units, from 20 up to 100. A stationary spatial pattern forms behind the leading wave front, whose wavelength is approximately 33 dimensionless units, i.e. 33 typical cell lengths. The wave front remains well defined, with a wave speed of 6.004 36, within 0.005% of the predicted speed. The parameters are: $D_l = D_m = D_n = 5$, $D_f = 100$, $D_c = 2.5$, $\alpha = 0.01$, $\beta = 5.0$, $\delta_c = 0.5$, $\delta_f = 2.0$, $\delta_l = 0.1$, $N = 1$, $I = 0.01$, $k_1 = 10.0$, $k_2 = 0.2$, $\sigma = 58$, $\xi = 2.8$.

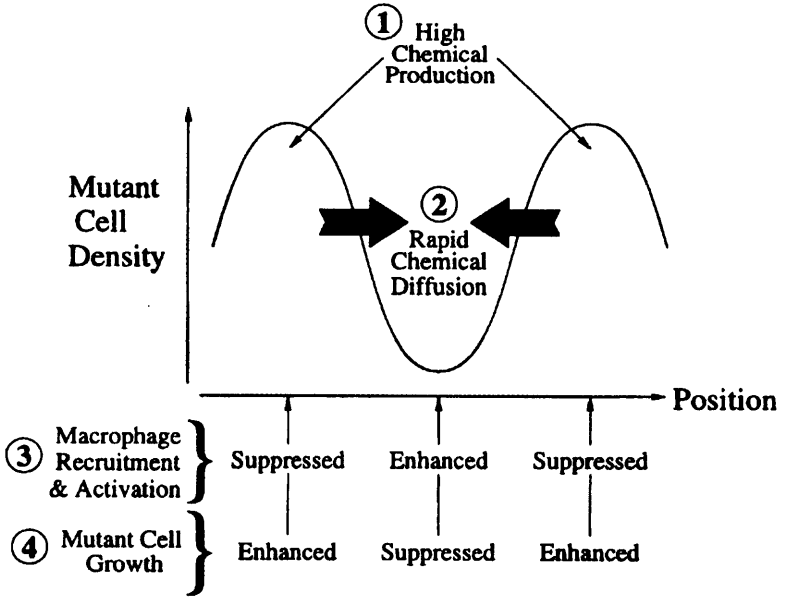

Fig. 5. An intuitive explanation for the development of spatial inhomogeneities within a tumour, due to interactions with macrophages. A locally elevated mutant cell density is reinforced by the consequently elevated chemical regulator production (step 1) – if the chemical diffuses sufficiently fast (step 2), then local macrophage recruitment and activation will be suppressed (step 3), and hence mutant cell growth enhanced (step 4). Correspondingly, nonlocal recruitment and activation of macrophages will be enhanced, and mutant cell growth suppressed.

the chemical regulator is the long-range inhibitor. Thus, an intuitive explanation for this spatial instability, illustrated in Fig. 5, is that given a local perturbation increasing the density of mutant cells, chemical regulator production will also increase locally. Then if the chemical diffuses fast enough, it will act nonlocally to activate macrophages to the tumouricidal state and to stimulate an additional influx of macrophages. This will suppress nonlocal mutant cell growth, whilst enhancing local mutant cell growth, due to the relative suppression of local macrophage activation, so that the original perturbation will grow in time. Thus it is the inclusion of chemical diffusion, which occurs at a much faster rate than random cell migration, that is responsible for this diffusion driven instability. The diffusion coefficient D_f for the chemical regulator is expected to be substantially larger than the random motility coefficients for cells, but we are not aware of data enabling precise values to be calculated. Such data would in fact be relatively easy to obtain via *in vitro* experiments, and our results suggest that this would be a valuable line of experimental investigation.

4.1. *Analytical study of pattern formation*

The first step to an analysis of the patterning phenomenon is to linearise the model (4) about the stable homogeneous steady state. A general perturbation can then be

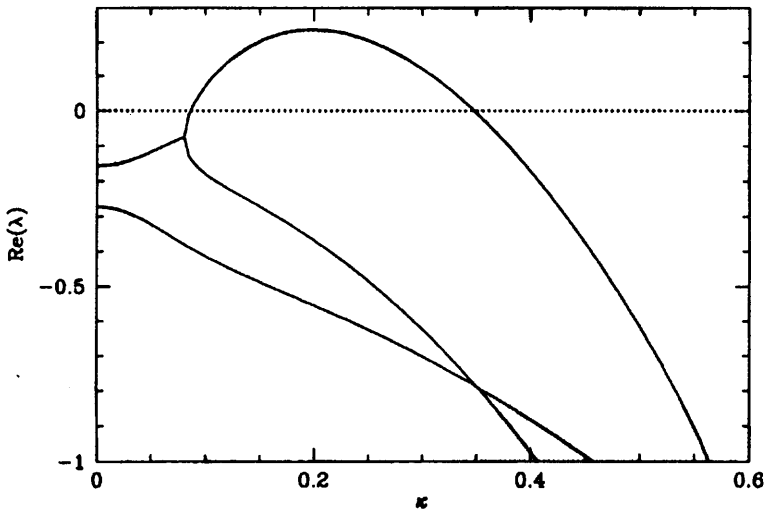

Fig. 6. Numerically calculated dispersion relation for the model (4), showing Re(λ) as the wave number κ varies. The different curves are for different eigenvalues. For κ between 0.09 and 0.345 the real part of one of the eigenvalues is positive, indicating that the homogeneous steady state is unstable to perturbations with those wave numbers. The fastest growing mode is approximately $\kappa = 0.2$, corresponding to a wavelength of 31 cell lengths, which compares well with the actual wavelength of 33 seen in the numerical simulation with the same parameters, shown in Fig. 4. The dispersion relation is calculated by finding the real part of the eigenvalues of the linearised system for κ varying upwards from zero in increments of 0.005.

expressed as a linear combination of spatial modes, and so substituting solutions proportional to $e^{i\kappa x+\lambda t}$ into the linearised equations and looking for nontrivial solutions gives the dispersion relation for the real part of λ (i.e. the growth rate) as a function of wave number κ. The homogeneous steady state is then stable to all spatial perturbations if $\mathrm{Re}(\lambda) < 0$ for all $\kappa \in \mathrm{R}$, while if $\mathrm{Re}(\lambda) > 0$ for some κ, then the mode corresponding to that wave number will grow exponentially in time, destabilising the homogeneous steady state.

Figure 6 illustrates the numerically calculated dispersion relation for a parameter set for which a range of wave numbers are unstable; Fig. 4 shows the corresponding numerical simulation of the partial differential equations. Although the wave front is moving, the pattern which grows behind the front is stationary in space, with a wavelength of 33 cell lengths. The wave number of the fastest growing mode in the dispersion relation is approximately $\kappa = 0.2$, giving a wavelength of 31 cell lengths, in good agreement with the above observation from numerical simulations.

To study the mechanisms underlying pattern formation in more detail, we consider a caricature model with only two variables. Such systems are more amenable to analysis, and an analytical expression for the critical diffusion coefficient for spatial instabilities can easily be derived.[36] Since the pattern formation is driven by the much faster diffusion of chemical regulators, it is essential to include the chemical explicitly in any caricature, and so the second variable should be equivalent to either

macrophages, or mutant cells. We consider a caricature model with mutant cells m and chemical regulator f, derived from the full equations by setting $\partial l/\partial t = \partial n/\partial t = \partial c/\partial t = 0$, and $D_l = D_n = D_c = \chi_l = 0$, and then solving for l, n and c in terms of m and f. Such a simplification is made considerably easier in this case by assuming the steady state is one of coexistence, so that $l + m + n = 1$. Indeed, without this assumption a quadratic would have to be solved for l, negating the algebraic simplicity of a caricature. The result is a simple model with mutant cell growth inhibited by the chemically regulated immune response, whose effect is modulated by terms representing macrophage influx, growth, death and the formation of complexes:

$$\frac{\partial m}{\partial t} = D_m \nabla^2 m + M(m, f)$$

$$\equiv D_m \nabla^2 m + m(\xi - 1) - \frac{\overbrace{k_1 I(1+\sigma f)}^{\text{influx}} fm}{\underbrace{\delta_l}_{\text{death}} - \underbrace{\alpha f}_{\text{growth}} + \underbrace{\frac{k_1 \delta_c f m}{k_2 + \delta_c}}_{\text{complex}}}, \tag{5a}$$

$$\frac{\partial f}{\partial t} = D_f \nabla^2 f + F(m, f) \equiv D_f \nabla^2 f + \beta m - \delta_f f\,. \tag{5b}$$

This model has an unstable "normal tissue" steady state $(m, f) = (0, 0)$, and two coexistence steady states which correspond precisely to those discussed in Sec. 3. As before, only one such coexistence state is non-negative, except within a very small region of parameter space. We denote the non-negative steady state, which is stable to homogeneous perturbations, by $(m, f) = (m_e, f_e)$. Differentiating $M(m, f)$ with respect to f shows that the strength of the immune response is an increasing function of the chemical regulator concentration, supporting our intuition that rapid diffusion of regulator away from regions of elevated mutant cell density causes a local reduction in the immune response, allowing mutant cell levels to rise further, whilst causing a nonlocal increase in mutant cell killing, reinforcing the perturbation. Other kinetic terms combine to give a Jacobian matrix which indicates a pure activator–inhibitor model, so that m and f will have solutions in phase, at least close to the primary pattern forming bifurcation at $D_f = D_f^c$.[15]

This critical value of the chemical regulator diffusion coefficient, for diffusion driven instability of the steady state $(m, f) = (m_e, f_e)$, is given analytically[36] by

$$D_f^c = D_m \frac{(M_m F_f - 2M_f F_m) + \sqrt{(2M_f F_m - M_m F_f)^2 - M_m^2 F_f^2}}{M_m^2} \tag{6}$$

and the critical wave number at the onset of instability is

$$\kappa^c = \sqrt{\frac{D_f^c M_m + D_m F_f}{2 D_f^c D_m}}, \tag{7}$$

where $M_m \equiv \partial M(m_e, f_e)/\partial m$ and similarly for M_f, F_m and F_f.

To investigate the validity of our caricature it is interesting to compare the values given by (6) for the caricature model, with D_f^c for the full model; this comparison is illustrated in Fig. 7. For the particular parameters used in this figure, the curves of D_f^c, for the caricature model and the full model, match almost exactly for small σ, but diverge significantly for σ greater than about 74. We studied this by plotting κ^c, the wave number at the onset of instability, and we found that the divergence in D_f^c is due to the full and caricature models becoming unstable to perturbations of different wave numbers, as illustrated in Fig. 7.

It is to be expected that whenever the real part of an eigenvalue for the caricature model passes through zero, the same will be true for the full model, but the opposite is not necessarily the case. This means that the first eigenvalue of the full model to pass through the imaginary axis (in the complex plane) may or may not coincide with a similar transition for the caricature. Hence, the curves of D_f^c

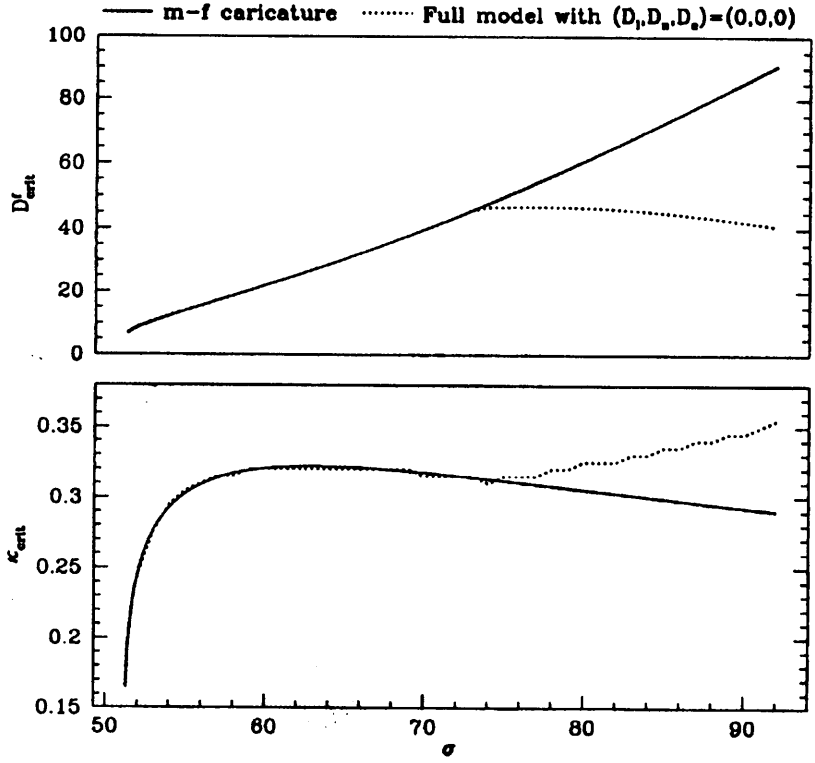

Fig. 7. A comparison of the critical diffusion coefficient D_f^c and the corresponding wave number κ_c, for the full (dotted curve) and caricature (full curve) models. For small σ, D_f^c and κ_c are the same for the two models, but at $\sigma \approx 74$, the critical wave numbers become different, along with D_f^c. The critical diffusion coefficient and wave number for the full model are calculated numerically, with the range of wave numbers discretised with an interval of 0.05. The corresponding values for the caricature model are given by (6) and (7). The parameters are: $D_m = 5$, $\alpha = 0.01$, $\beta = 5.0$, $\delta_c = 0.5$, $\delta_f = 2.0$, $\delta_l = 0.1$, $N = 1$, $I = 0.01$, $k_1 = 10.0$, $k_2 = 0.2$, $\xi = 2.8$, $D_l = D_n = D_c = 0$.

match exactly when these transitions do coincide, but diverge otherwise. Figure 8 illustrates how, for σ such that the full model and caricature D_f^c curves are distinct, the full model initially becomes unstable to perturbations at a smaller value of D_f than the caricature, but as the caricature model bifurcates to patterned solutions, the full model, as expected, also has an eigenvalue with zero real part at that point. Of course, this has no implications for the stability of the full model.

We have shown that the caricature model is a good approximation to the full model for the purposes of studying bifurcations to spatial instability, at least for small σ, but differences in the nonlinear terms mean that, away from the bifurcation, the comparison breaks down. In particular, the absence in the caricature model (5) of terms limiting mutant cell growth (modelling crowding) means that initially small spatial oscillations continue to grow, and become unbounded. Thus the caricature model is a useful tool only in the linear regime.

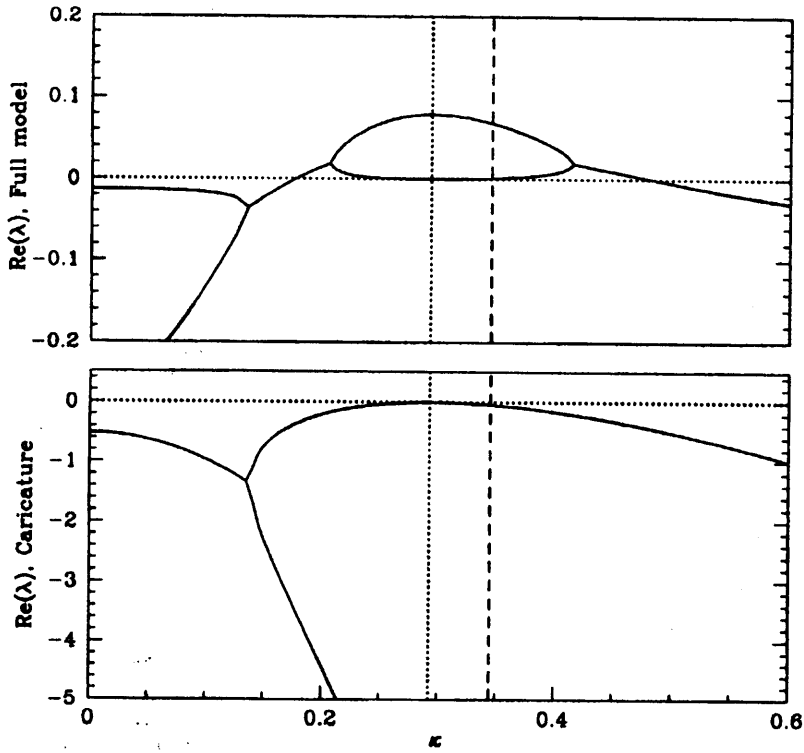

Fig. 8. Dispersion relations for the full and caricature models, close to the onset of spatial instability in the caricature model. When the full model and caricature D_f^c curves are distinct, the full model initially becomes unstable to perturbations at a smaller value of D_f than the caricature, but as the caricature model bifurcates to patterned solutions, the full model, as expected, also has an eigenvalue with zero real part. The dashed vertical line indicates the critical wave number for the initial instability in the full model, and the dotted line indicates the critical wave number for the caricature model. The other model details and parameters are as in Fig. 7, with $D_f = 85$.

5. Including the Effects of Chemotaxis

In 1983, Bottazzi *et al.*[10] identified a monocyte chemoattractant which is released by various human and mouse tumours. Subsequent work has demonstrated a number of chemoattractants,[49,51] and the ability to synthesise and/or purify these and other macrophage chemoattractants has enabled detailed quantitative comparisons of *in vitro* chemotactic activity.[48] It is to be expected that tumours inducing high levels of chemotactic activity *in vitro* would correspond to *in vivo* tumours with high levels of macrophage infilitration, and this has indeed been shown to be the case.[50] Moreover, the majority of monocyte chemotactic activity does not derive from stromal or lymphoreticular cells (i.e. non-malignant cells),[9] and is independent of specific T-cell immunity,[50] so that the main source of chemoattractants *in vivo* is tumour

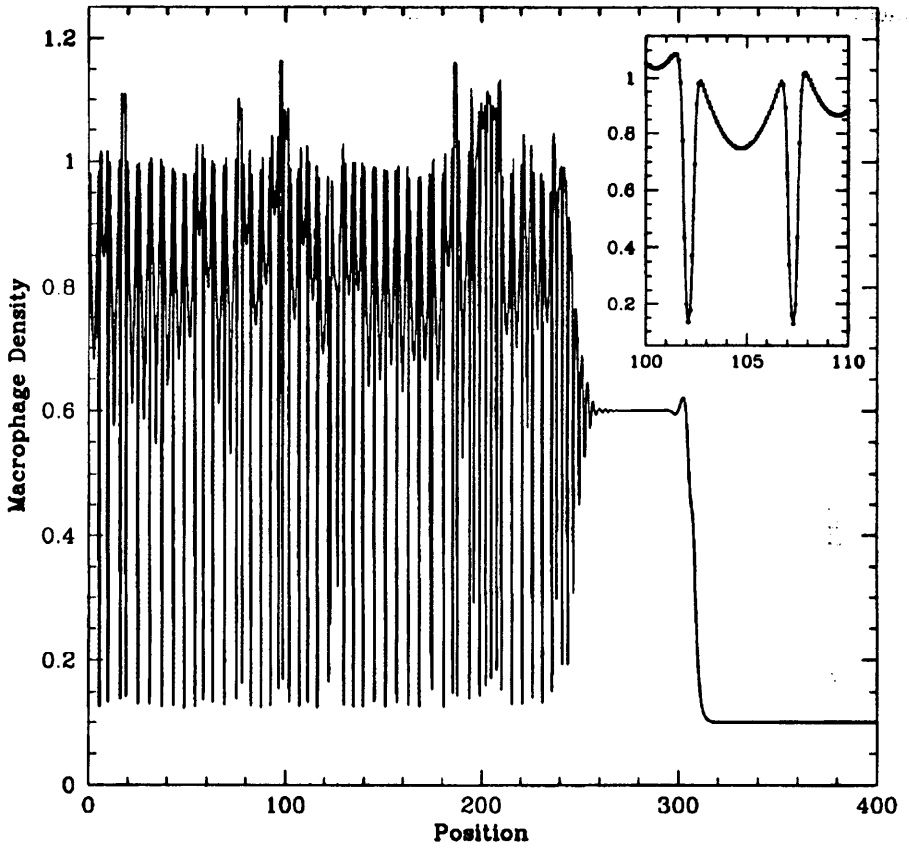

Fig. 9. Numerical simulation of the model (4) including chemotaxis. A travelling wave evolves from a seed of one mutant cell at the origin, but behind the wave front the solution is irregular, compared with the regular patterns seen without chemotaxis in Sec. 4. The magnification shows the individual grid points of the finite difference numerical scheme, illustrating the spatial resolution of the solution. The parameters are: $D_l = D_m = D_n = 0.01$, $D_f = 5.0$, $D_c = 0.005$, $\chi_l = 0.5$, $\alpha = 0.01$, $\beta = 5.0$, $\delta_c = 0.5$, $\delta_f = 2.0$, $\delta_l = 0.1$, $N = 1$, $I = 0.01$, $k_1 = 10.0$, $k_2 = 0.2$, $\xi = 2.0$, $\sigma = 58$.

cells themselves. In this section we discuss the effect of including macrophage chemotaxis in our model.

The basic solution form, in which a tumour grows from an original mutation site, is not changed by the introduction of chemotaxis. Thus if the steady state behind the wave is stable to spatial perturbations, then the solution is unchanged except for minor alterations in the shape of the wave front. However, the inclusion of chemotaxis in the model can stabilise the spatially homogeneous steady state when this is unstable to perturbations in the absence of chemotaxis. Numerical investigation shows that as the chemotaxis coefficient is increased, the peak in the dispersion relation moves down, so that wave numbers whose corresponding eigenvalues had a positive real part no longer do so. This means that as χ_l increases, the value of the chemical diffusion coefficient at which spatial instabilities appear, denoted D_f^c, also increases.[39]

In contrast to these relatively minor effects, the inclusion of chemotaxis can in some cases give a qualitatively new type of behaviour, namely irregular spatio-temporal oscillations behind the wave front. Figure 9 shows the result of one such simulation. Behind the wave front the solution does not settle down in time or space. Initially we wondered whether these results were simply due to numerical instability, but refining the spatial mesh retained the same qualitative form, and the resolution was sufficiently high that what may have looked like noisy spikes were seen to be smooth curves. This is clear in Fig. 9 where individual points have been plotted in a magnified section, to show how clearly resolved the solution is.

Although there is ample evidence of spatial heterogeneity in tumours, detailed spatio-temporal data is unavailable. Nevertheless, it does seem plausible that spatio-temporal variations will occur given the dynamic nature of the various processes involved in tumour progression. Simulations such as that illustrated in Fig. 9 obviously exclude many processes occurring in real tumours, making detailed correlation between simulations and data unrealistic; however, our results do suggest that spatiotemporal irregularity should be expected in practice for appropriate levels of macrophage chemotaxis.

5.1. *Bifurcation routes to spatiotemporal irregularity*

In order to gain insight into the mathematical nature of this phenomenon, simulations were carried out on small finite domains with random initial conditions. Domain length is often a useful bifurcation parameter: for example on a finite domain the wavelength of a Turing pattern is determined by its length, and there have been extensive studies of transitions to irregularity as the domain size is varied, including work on the Ginzburg–Landau equation[35,47] and oscillatory reaction–diffusion equations.[43] The application of such ideas to wave fronts is motivated by the idea that the front can be seen as a moving boundary, changing the domain size. In terms of the tumour biology, the patterning and oscillations of the model only occur on the domain of the growing tumour, so that treating the invading front of mutant cells in this way has a clear interpretation.

It is the long-term behaviour of the solutions behind the wave that is of interest, and this technique enables the detailed characterisation of the types of solution that may be expected. We describe this study for one specific parameter set: $D_l = D_m = D_n = 0.01$, $D_f = 5$, $D_c = 0.005$, $\chi_l = 0.5$, $\alpha = 0.01$, $\beta = 5.0$, $\delta_c = 0.5$, $\delta_f = 2.0$, $\delta_l = 0.1$, $N = 1$, $I = 0.01$, $k_1 = 10.0$, $k_2 = 0.2$, $\sigma = 58$, $\xi = 2.0$. Note that the choice of this particular set of parameters is purely arbitrary within the scope of our order of magnitude estimates, which were given in Refs. 38 and 39. However, less detailed numerical investigations confirm that irregular solutions still arise for other parameters.

At small domain lengths (we started at a domain length of 2.5), solutions evolved from random initial conditions to a stationary spatial pattern. As the domain size was increased, the solution changed in parallel; this is expected since the domain size dictates the allowable wave numbers of the spatial instability. Finally, at a size of 5.0 the solutions failed to settle down to steady patterns, oscillating instead with a period of about 864 dimensionless time units. The natural next step is to determine precisely where the transition from stationary to oscillating solutions occurs. However, this is not so straightforward, since any change of grid size will slightly alter the dynamics of the simulation, and change the results. The first simulations on a finite domain were done with a grid spacing of 0.025, dictating the same smallest step in domain size to avoid compromising the results. It was while attempting to find the transition that we found that both the oscillatory and the steady solutions could stably coexist, possibly indicating a subcritical Hopf bifurcation. In addition to this we found that upon a further increase in domain size to 5.2, the oscillations no longer occurred. At this point it became clear that a primitive form of parameter continuation was needed to follow the bifurcating branches of solutions as the domain length was changed. This was achieved by substituting the solution from the previous simulation and scaling it to fit the new domain length, so that by starting close to what was stable, the solution should remain on the same stable branch. The results of this continuation are shown in Figure 10. This suggests that one stationary pattern is always stable, but that as the domain size increases an oscillatory state also becomes stable, until what appears to be a Hopf bifurcation point is passed, and the oscillatory state becomes steady; this new steady pattern is different to the original steady pattern, which still stably coexists itself. Following the continuation from (a) to (f) in the figure illustrates how this leads to hysteresis, and Fig. 11 shows how the nature of the pattern differs, according to which solution branch is followed. Figure 12 shows temporal solutions at four of the labelled points, clearly illustrating the regular periodic nature of the oscillatory solutions, and the coexistence at the same domain length of distinct oscillatory and stationary states.

It is interesting to note that, for our particular choice of parameters, the oscillations are not due to the spatial modes of the original solution having nonzero imaginary parts, which would also lead to oscillations — this is clear from careful checking of the dispersion relation. For some other parameter sets, growing spatial

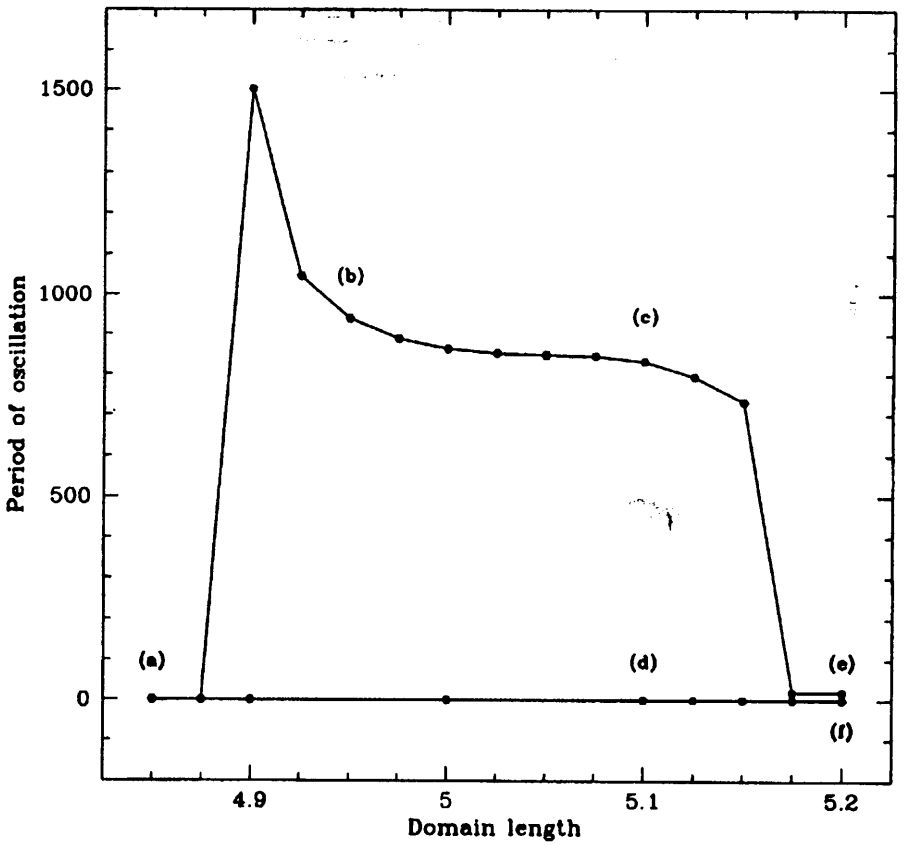

Fig. 10. The structure of the first bifurcation as the domain length increases. The period of oscillation, as calculated from numerical simulations, is plotted against the domain length. Starting at (e), $L = 5.2$, with a stable steady pattern, as the domain length is decreased, it seems that there is a supercritical Hopf bifurcation between 5.175 and 5.15, causing the steady pattern to start to oscillate as at (c), $L = 5.1$. Decreasing further through (b), $L = 4.95$, the period of oscillation increases, until the continuation of the oscillatory solution becomes unstable, and a steady pattern, as at (a), $L = 4.85$, becomes stable. Upon increasing the domain length again, however, the solutions do not return to the oscillating branch. Instead the steady pattern remains stable, for example at (d), $L = 5.1$. At (f), $L = 5.2$, the stable steady pattern is different from the initial pattern at (e), indicating hysteresis. A primitive parameter continuation was used, by rescaling the previously calculated stable solution to fit the new domain length, adding a small perturbation, and then using the result as the initial condition. Note that the details of the simulation such as grid size can affect the point at which oscillations appear, so that they must be kept constant.

modes do have complex eigenvalues, but the above observation indicates that this is not a requirement for oscillatory solutions. Such solutions are also not due to any oscillatory behaviour in the kinetics, in contrast to work by others such as Dunbar,[16] Sherratt *et al.*,[42,44] and Merkin,[34] which is concerned with reaction–diffusion systems whose kinetics are oscillatory in the absence of spatial variations.

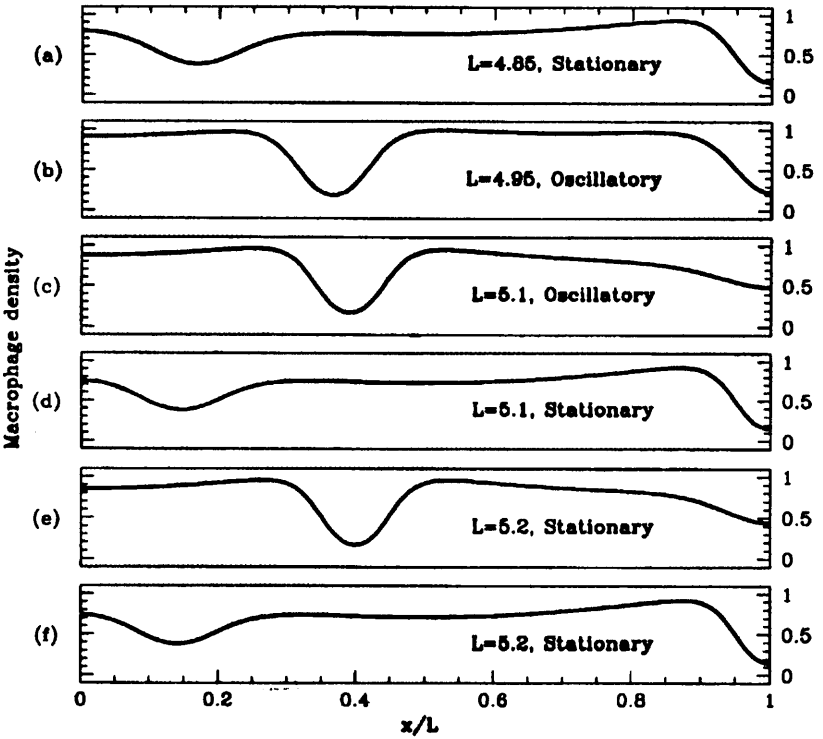

Fig. 11. Numerically calculated solution at time 5000 showing spatial structure as the domain length varies, illustrating two types of pattern which coexist stably, one of which can oscillate. The letters correspond to the points on the bifurcation diagram of Fig. 10. In particular, (e) and (f) illustrate the coexistence at the same domain length of two types of steady pattern, the first of which bifurcates to give oscillations, and the second remains stable. The domains are rescaled to 1 for ease of comparison.

In this model for the macrophage–tumour interaction, it is the pattern itself which becomes unstable, apparently through a Hopf bifurcation, to a new solution branch, while the homogeneous steady state from which the pattern bifurcated remains stable to homogeneous perturbations. It seemed plausible that this bifurcation may repeat at integer multiples of the critical domain length, and numerical solutions provided evidence for this.

With regard to the simulations of tumour growth on infinite domains, as already discussed, the wave front can be regarded as a moving boundary, so that effectively the domain is a finite but growing one. This could explain the irregular wakes seen behind travelling wave fronts in simulations on large domains — as the wave progresses, oscillatory solutions continually appear and disappear as the effective domain length moves through a series of bifurcation points. Note that the long-term behaviour of the solutions on a finite domain is not irregular, but rather is oscillatory with a fixed period. In contrast, when considering the travelling wave situation the behaviour observed is in effect permanently transient.

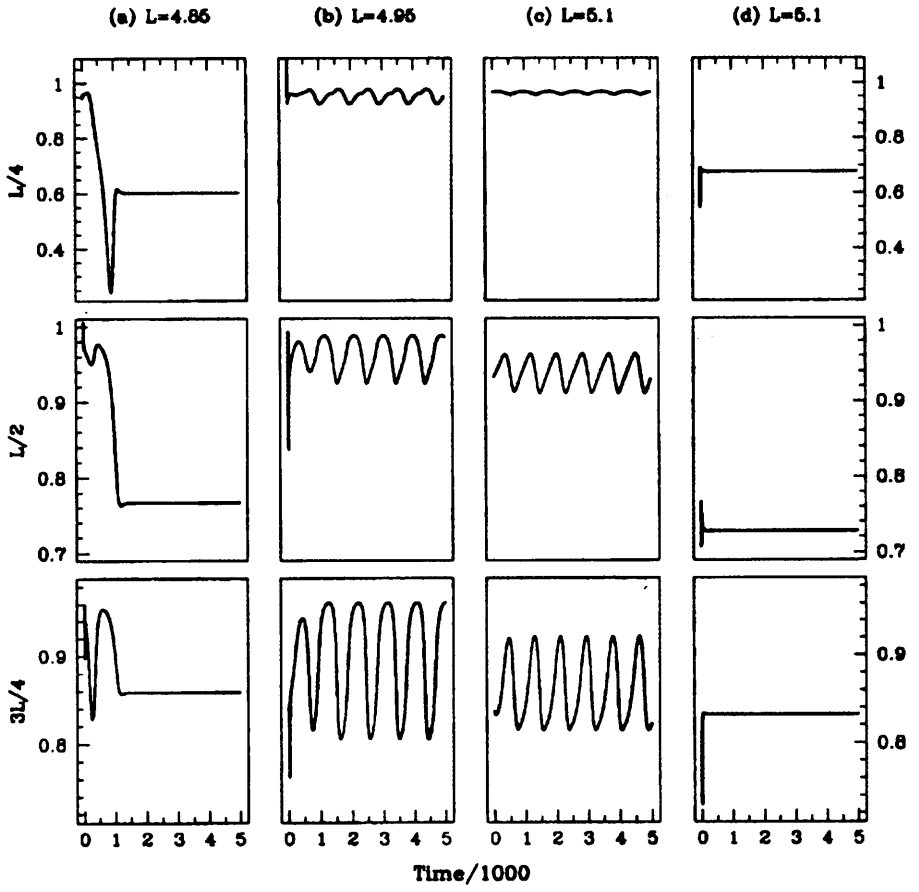

Fig. 12. Examples of numerically simulated spatially heterogeneous solutions, for four different domain lengths corresponding to the labelled points in the bifurcation diagram of Fig. 10. The macrophage density is plotted against time for three different points in the domain. For (a) and (d) the solution quickly settles down to a steady pattern, but the regular temporal oscillations indicated in the bifurcation diagram are clear for cases (b) and (c). Note that (c) and (d) clearly demonstrate the coexistence at the same domain length of distinct oscillatory and stationary states.

6. Numerical Simulations in Two Dimensions

So far we have considered solutions in one space dimension only, but of course real tumours reside in a three-dimensional tissue. For any mathematical model, the range of potential solution behaviours is much greater in higher dimensions, and while numerical solution of the equations in three dimensions would be too computationally intensive for our current resources, two-dimensional simulations are feasible, and show a number of features of interest. Perhaps a central theme in the biological background to this work, and indeed in much of tumour biology, is the heterogeneity between and within tumours. It is that within tumours that is the focus of this paper, and we have demonstrated a possible mechanism for the

development of spatial heterogeneity. The more realistic two-dimensional setting and the possibility of still greater complexity, such as an instability of the wavefront itself, is the focus of interest in an investigation of two-dimensional solutions.

The dispersion relation as calculated in Sec. 4, and illustrated in Fig. 6, is still valid, so that whenever patterns appear in one dimension they will also appear in two, but the precise nature of those patterns requires investigation. In one dimension the unstable wave number κ is a scalar, and a corresponding instability can only give rise to a single pattern, but in two dimensions the corresponding wave number (κ_x, κ_y) is two-dimensional, with $\kappa = \{\kappa_x^2 + \kappa_y^2\}^{1/2}$. If one of κ_x and κ_y is zero, then the pattern will be just simple stripes, but if they are both nonzero, then the pattern will be two-dimensional, tiling the plane. This introduces the possibility of more than one pattern being stable for a given parameter set, depending on the domain and initial conditions.

The model equations were solved in two dimensions using an alternating direction implicit method. This means that each time step consists of an explicit half-time step in the x direction and an implicit half-time step in the y direction, and then similar half-time steps exchanging explicit for implicit and vice versa. Figure 13 shows a shaded plot of the macrophage density that develops following a localised introduction of mutant cells into normal tissue, in a case in which there is no macrophage chemotaxis ($\chi_l = 0$). A circular travelling wave is established, behind which the tumour steady state is unstable to spatial perturbations, which

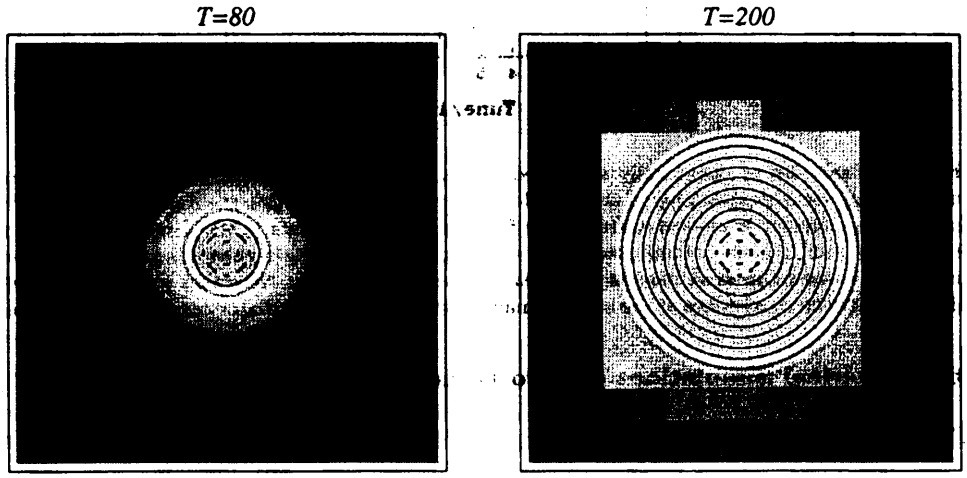

Fig. 13. Numerical simulation in two dimensions, showing the macrophage density after 80 and 200 dimensionless time units of evolution from a single unit seeding region with a mutant cell density of 1, located at the centre of the domain. Macrophage density is represented on a grey scale, with darker colouring indicating lower cell density. Behind the wavefront a spatial perturbation grows to form a target pattern, although at the centre this pattern has broken down. The structure at the centre is invariant in time, and is likely to be due to the effect of high curvature. The domain size is 2000 × 2000, and the parameters are $D_l = D_m = D_n = 5$, $D_f = 500$, $D_c = 2.5, \chi_l = 0$, $\alpha = 0.01$, $\beta = 5.0$, $\delta_c = 0.5$, $\delta_f = 2.0$, $\delta_l = 0.1$, $N = 1$, $I = 0.01$, $k_1 = 10.0$, $k_2 = 0.2$, $\sigma = 40$, $\xi = 2.0$.

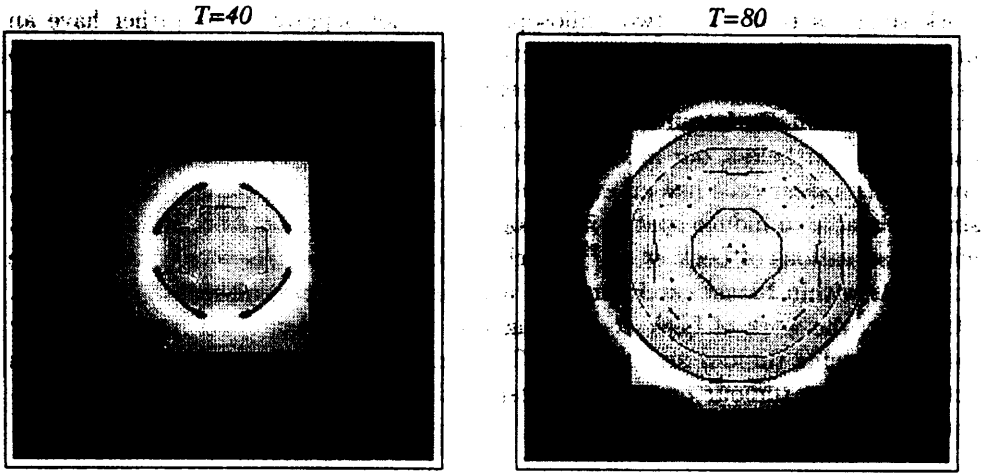

Fig. 14. Numerical simulation in two dimensions, with macrophage chemotaxis. In contrast to Fig. 13, the solution behind the wavefront is irregular in space and time. The domain size and parameters are as in Fig. 13, except for $D_l = 40$, $D_f = 1\,0000$, $\chi_l = 2\,000, \sigma = 58$, and $\xi = 2.8$.

leads to the formation of a stationary target pattern. The concentric rings in the circular geometry of the simulation correspond to stripes in a planar geometry; the break up of the pattern at the centre seems likely to be due to curvature effects. Numerical simulations for the same parameters, but on a finite rectangular domain with randomly generated initial conditions, indicate that for the parameters used in the figure, both spotted and striped patterns stably coexist, with the initial conditions determining which state is reached. This is a well-known phenomenon away from a primary Turing bifurcation[36]; note that sufficiently close to a Turing bifurcation, only one of the striped and spotted patterns can be stable.[17] However, our simulations indicate that, for the parameters in Fig. 13, stripes always develop in the simulation of the growing tumour.

As expected from the results on one-dimensional behaviour, the inclusion of macrophage chemotaxis ($\chi_l \neq 0$) results in much more complex patterns developing within the tumour; an example is illustrated in Fig. 14; however, we have not attempted a detailed study of such patterns. In real tumours, any irregularities due to chemotaxis would be increased by the effects of environmental noise, so that the results illustrated in Figs. 13 and 14 are not expected to represent real situations that might arise in practice. The essential implication of our results is rather that macrophage–tumour cell interactions can act as a first step in the initiation of both spatial and spatiotemporal heterogeneity.

7. Discussion

The ability of the immune system to spontaneously eliminate tumours was widely debated in the '50s and '60s. In more recent years, attention has switched to the more complex regulatory effects of the immune system on tumour progression. Our

work suggests that these two philosophies are not separate, but rather have an important overlap. Our model predicts that macrophages are unable to spontaneously eliminate whole tumours, in keeping with the conventional view that without intervention, the immune system is an ineffective weapon against the majority of cancers. Nevertheless, our model predicts that the ability of macrophages to selectively kill tumour cells has an extremely significant effect on tumour development, since it is able to induce spatial inhomogeneities. This new prediction is consistent with observations of Leek *et al.*,[29] which demonstrate the existence of macrophage hot-spots within breast carcinomas, in a manner highly reminiscent of our results. Moreover, the work of Leek *et al.*[29] suggests that these hot-spots may play a key role in inducing tumour angiogenesis. This implies that high macrophage densities actually favour tumour progression, despite their anti-tumour activities, an observation made previously by Lewis *et al.*[30] Our work suggests that this anti-tumour activity may nevertheless be crucial in establishing the spatial structure that is able, later, to induce angiogenesis.

At appropriate levels of macrophage chemotaxis, we have demonstrated spatio-temporal irregularities in the model solution. Our numerical bifurcation study suggests that the mechanism by which these occur is that a stationary spatial (Turing) pattern becomes unstable via a Hopf bifurcation, while the homogeneous equilibrium from which the Turing pattern bifurcated remains kinetically stable. To the best of our knowledge, this is a new mechanism, which can only occur far from Turing bifurcation, making analytical investigation an extremely hard challenge.

Experimental investigation of the predictions of our model is potentially possible using cell spheroid assays, which could in principle be seeded with macrophage cells. This line of inquiry provides the exciting possibility of providing a detailed, quantitative link between the results of a model of the type we are considering, and experimental data. This would provide a natural route towards detailed applications of our model to *in vivo* tumour dynamics.

Acknowledgments

This work was supported in part by the following grants: an earmarked studentship from the Engineering and Physical Sciences Research Council (MRO), grant GR/L41967 from the Engineering and Physical Sciences Research Council, and a grant (scheme 3) from the London Mathematical Society. We would like to thank Nigel Burroughs, John Dallon, Claire Lewis, Mark Lewis and Abbey Perumpanani for helpful discussions.

References

1. J. A. Adam, *A simplified mathematical model of tumor growth*, *Math. Biosci.* **81** (1986) 229–244.
2. J. A. Adam, *The dynamics of growth-factor-modified immune response to cancer growth: One-dimensional models*, *Math. Comput. Modelling* **17** (1993) 83–106.
3. J. A. Adam and N. Bellomo, **A Survey of Models for Tumor-Immune System Dynamics** (Birkhäuser, 1997).

4. A. Albert, M. Freedman and A. S. Perelson, *Tumors and the immune system: The effects of a tumor growth modulator, Math. Biosci.* **50** (1980) 25–28.
5. P. Allavena, M. Grandi, M. D. Incalci, O. Geri, F. C. Guiliani and A. Mantovani, *Human tumor cell lines with pleiotropic drug resistance are effectively killed by interleukin-2 activated monocytes, Internat. J. Cancer* **40** (1987) 104–107.
6. P. Allavena, F. Peccatori, D. Maggioni, M. Sironi, N. Colombo, A. Lissoni, A. Galazka, W. Meiers, C. Mangioni and A. Mantovani, *Intraperitoneal recombinant γ-interferon in patients with recurrent ascitic ovarian carcinoma: Modulation of cytotoxicity and cytokine production in tumor-associated effectors and major histocompatibility antigen expression on tumor cells, Cancer Res.* **50** (1990) 7318–7323.
7. R. Andreesen, C. Scheibenbogen, W. Brugger, S. Krause, H. Leser, H. Engler and G. Löhr, *Adoptive transfer of tumor cytotoxic macrophages generated in vitro from circulating blood monocytes: A new approach to cancer immunotherapy, Cancer Res.* **50** (1990) 7450–7456.
8. B. Bottazzi, E. Erba, N. N. Nobili, F. Fazioli, A. Rambaldi and A. Mantovani, *A paracrine circuit in the regulation of the proliferation of macrophages infiltrating murine sarcomas, J. Immunol.* **144** (1990) 2409–2412.
9. B. Bottazzi, P. Ghezzi, G. Taraboletti, M. Salmona, N. Colombo, C. Bonnazzi, C. Mangioni and A. Mantovani, *Tumor-derived chemotactic factor(s) from human ovarian carcinoma: Evidence for a role in the regulation of macrophage content of neoplastic tissues, Internat. J. Cancer* **36** (1985) 167–173.
10. B. Bottazzi, N. Polentarutti, R. Acero, A. Balsari, D. Boraschi, P. Ghezzi, M. Salmona and A. Mantovani, *Regulation of the macrophage content of neoplasms by chemoattractants, Science* **220** (1983) 210–212.
11. A. C. Burton, *Rate of growth of solid tumours as a problem of diffusion, Growth* **30** (1966) 159–176.
12. H. M. Byrne and M. A. J. Chaplain, *Growth of nonnecrotic tumors in the presence and absence of inhibitors, Math. Biosci.* **130** (1995) 151–181.
13. M. A. J. Chaplain and B. D. Sleeman, *A mathematical model for the production and secretion of tumor angiogenesis factor in tumors, IMA J. Math. Appl. Med. Biol.* **7** (1990).
14. M. A. J. Chaplain and A. M. Stuart, *A model mechanism for the chemotactic response of endothelial cells to tumor angiogenesis factor, IMA J. Math. Appl. Med. Biol.* **10** (1993) 149–168.
15. R. Dillon, P. K. Maini and H. G. Othmer, *Pattern formation in generalized turing systems I. steady-state patterns in systems with mixed boundary conditions, J. Math. Biol.* **32** (1994) 345–393.
16. S. R. Dunbar, *Traveling waves in diffusive predator-prey equations — periodic orbits and point-to-periodic heteroclinic orbits, SIAM J. Appl. Math.* **46** (1986) 1057–1078.
17. B. Ermentrout, *Stripes or spots — nonlinear effects in bifurcation of reaction-diffusion equation on the square, Proc. R. Soc. Lond.* **A434** (1991) 413–417.
18. J. J. Esgro, P. Whitworth and I. J. Fidler, *Macrophages as effectors of tumor immunity, Immun. Allergy Clin. N. Am.* **10** (1990) 705–729.
19. I. J. Fidler and E. S. Kleinerman, *Therapy of cancer metastasis by systemic activation of macrophages: From the bench to the clinic, Res. Immun.* **144** (1993) 284–287.
20. R. A. Fisher, *The wave of advance of advantageous genes, Ann. Eugenics* **73** (1937) 353–369.
21. J. Folkman, *Angiogenesis in cancer, vascular, rheumatoid and other disease, Nature Med.* **1** (1995) 27–31.
22. H. P. Greenspan, *Models for the growth of a solid tumour by diffusion, Stud. Appl. Math.* **51** (1972) 317–340.

23. K. Groebe and W. Mueller-Klieser, *Distribution of oxygen, nutrient and metabolic waste concentrations in muticellular spheroids and their dependence on spheroid parameters, Eur. J. Biophys.* **19** (1991) 169–181.
24. T. A. Hamilton and D. O. Adams, *Mechanisms of macrophage-mediated tumor injury*, in **Tumor Immunology — Mechanisms, Diagnosis, Therapy**, eds. W. den Otter and E. J. Ruitenberg (Elsevier, 1987), pp. 89–107.
25. J. R. Hiernaux and R. Lefever, *Population dynamics of tumors attacked by immunocompetent killer cells*, **Theoretical Immunology**, ed. A. S. Perelson (Addison-Wesley, 1988), Vol. 2, pp. 19–36.
26. N. Jonjic, S. Alberti, S. Bernasconi, G. Peri, P. Jilek, A. Anichini, G. Parmiani and A. Mantovani, *Heterogeneous susceptibility of human-melanoma clones to monocyte cytotoxicity — role of ICAM-1 defined by antibody blocking and gene transfer, Eur. J. Immun.* **22** (1992) 2255–2260.
27. V. A. Kuznetsov, *Harpoon model for cell–cell adhesion and recognition of target cells by the natural killer cells, J. Theor. Biol.* (1996) 321–342.
28. V. A. Kuznetsov, V. P. Zhivoglyadov and L. A. Stepanova, *Kinetic approach and estimation of the parameters of cellular interaction between the immunity system and a tumor, Arch. Immun. Theory. Exp.* **41** (1993) 21–31.
29. R. D. Leek, C. E. Lewis, R. Whitehouse, M. Greenall, J. Clarke and A. L. Harris, *Association of macrophage infiltration with angiogenesis and prognosis in invasive breast carcinoma, Cancer Res.* **56** (1996) 4625–4629.
30. C. E. Lewis, R. Leek, A. Harris and J. O. D. McGee, *Cytokine regulation of angiogenesis in breast cancer — the role of tumor-associated macrophages, J. Leukoc. Biol.* **57** (1995) 747–751.
31. K. F. Mace, M. J. Ehrke, K. Hori, D. L. Maccubbin and E. Mihich, *Role of tumor necrosis factor in macrophage activation and tumoricidal activity, Cancer Res.* **48** (1988) 5427–5432.
32. A. Mantovani, *Tumour-associated macrophages, Curr. Opin. Immun.* **2** (1990) 689–692.
33. A. Mantovani, B. Bottazzi, F. Colotta, S. Sozzani and L. Ruco, *The origin and function of tumor-associated macrophages, Immun. Today* **13** (1992) 265–270.
34. J. H. Merkin, V. Petrov, S. K. Scott and K. Showalter, *Wave-induced chemical chaos, Phys. Rev. Lett.* **76** (1996) 546–549.
35. H. T. Moon, P. Huerre and L. G. Redekopp, *Transitions to chaos in the Ginzburg–Landau equation, Physica* **D73** (1983) 135–150.
36. J. D. Murray, **Mathematical Biology** (Springer-Verlag, 1991).
37. C. O'Sullivan and C. E. Lewis, *Tumor-associated leukocytes — friends or foes in breast-carcinoma, J. Path.* **172** (1994) 229–235.
38. M. R. Owen and J. A. Sherratt, *Modelling the macrophage invasion of tumours: effects on growth and composition, IMA J. Math. Appl. Biol.* **15** (1998) 165–185.
39. M. R. Owen and J. A. Sherratt, *Pattern formation and spatiotemporal irregularity in a model for macrophage–tumour interactions, J. Theor. Biol.* **189** (1997) 63–80.
40. A. J. Perumpanani, J. A. Sherratt, J. Norbury and H. M. Byrne, *Biological inferences from a mathematical model for malignant invasion, Invasion & Metastasis* **16** (1996) 209–221.
41. A. Sampson-Johannes and J. A. Carlino, *Enhancement of human monocyte tumoricidal activity by recombinant M-CSF, J. Immun.* **141** (1998) 3680–3686.
42. J. A. Sherratt, *Irregular wakes in reaction-diffusion waves, Physica* **D70** (1994) 370–382.
43. J. A. Sherratt, *Unstable wavetrains and chaotic wakes in reaction-diffusion systems of λ–ω type, Physica* **D82** (1995) 165–179.